Hindawi
Journal of Chemistry
Volume 2022, Article ID 5766269, 10 pages
https://doi.org/10.1155/2022/5766269

Research Article

Catalytic Hydrothermal Carbonization of Avocado Peel

Lien Thi Tran, Minh Quang Nguyen, Ha Trong Hoang, Hoang Tien Nguyen, and Thu Ha Thi Vu

National Key Laboratory for Petrochemical and Refinery Technologies, 2 Pham Ngu Lao Street, Hanoi, Vietnam

Correspondence should be addressed to Thu Ha Thi Vu; ptntd2004@yahoo.fr

Received 11 July 2022; Revised 8 September 2022; Accepted 13 September 2022; Published 7 October 2022

Academic Editor: Samuel Lalthazuala Rokhum

The hydrothermal carbonization (HTC) of avocado peel was investigated by varying the reaction temperature, reaction time, and catalyst/feedstock ratio. After the HTC process, there was a drastic change in both the structure and chemical composition of the hydrochar compared to the feedstock. This modification aids hydrochar's improved fuel characteristics, as seen by a drop in the H/C and O/C ratios, as well as an increase in fixed carbon content. The higher heating value (HHV) increased in the feedstock to a maximum value of 27.15 $MJ \cdot kg^{-1}$, corresponding to hydrochar, which is obtained at an optimized condition. Notably, the HHV and carbon content of the noncatalytic sample are only higher than those of the feedstock but lower than those of the samples surveyed. The combustion behavior and thermal characteristics of hydrochars show that the HTC of the avocado peel in the presence of $FeCl_3$ catalyst introduces a possible direction of application in converting agro-industrial by-products into fuel.

1. Introduction

Persea americana, also known as avocado, originated in Mexico and Central America and is now widely cultivated in tropical regions, for example, Vietnam. Avocados are highly valued and used for a variety of applications, including fresh fruit, nutritional supplements, oil extraction, and especially in the cosmetic industry due to their high nutritious content. The rapid growth of factories generates a large amount of organic waste, consisting mainly of avocado peels and seeds. Normally, these agro-industrial byproducts are handled by traditional methods such as landfilling or composting, which, however, have various weaknesses such as stench, waste of area, and time-consuming biodegradation processes. Meanwhile, avocado peels and seeds are a source of lignocellulosic biomass with major components including cellulose, hemicelluloses, and lignin, have a high content of carbon, and produce a lot of value if handled properly [1–3]. Some preliminary studies aimed at utilizing by-products for processing into value-added products have been conducted, but the pyrolysis method is mainly used [4–7]. These studies all obtained activated carbon with high porosity, large specific surface area, and good adsorption capacity for application in dyeing wastewater treatment [4, 5] or phenol removal [6]. Palma et al. [7] synthesized activated carbon from avocado peel by pyrolysis at 900°C for 65 minutes. The obtained carbonaceous material had a specific surface area of 87.52 $m^2 \cdot g^{-1}$ and a mesopore volume of 74%, capable of adsorption and removal of some basic dyes from aqueous solutions. A cheap and renewable bioadsorbent is produced through saponification of the avocado peel with NaOH [8]. This bioadsorbent is proven to be able to eliminate organic dyes and heavy metal ions from wastewater.

In recent years, hydrothermal carbonization (HTC) has been considered one of the most popular biomass thermochemical conversion methods to obtain high-value-added products from biomass wastes. Compared with other traditional techniques such as pyrolysis, the HTC process possesses many advantages, such as mild reaction conditions (generally 180–350°C, most commonly performed at a temperature of 180–250°C); reducing carbon dioxide emissions; and most importantly, the HTC process allows the conversion of wet biomass without pre-drying [9–11]. This allows the utilization of a wide range of biomass with a high content of water such as fruit wastes [12, 13], aquatic plants [14, 15], or agricultural byproducts [16–20].

The presence of ions and metal particles has been proven in numerous studies to have a substantial impact on the composition and structural morphology of the hydrochar produced by the HTC process [21, 22]. Furthermore, for starch and cellulose, the HTC process could be accelerated by boosting water dehydration, condensation, and carbonization in the presence of metal ions (Fe^{2+}, Ag^{+}) [23, 24]. The influence of iron salts on the HTC process of α-cellulose was also well studied by Bee et al. [25]. Another Lewis acid, $ZnCl_2$, is used in the HTC of glucose with the aim of facilitating the dehydration reaction [26]. The result is that a carbon material has a large surface area of up to 650 $m^2 \cdot g^{-1}$ and a typical aerogel structure without undergoing supercritical CO_2 drying.

However, to the best of our knowledge, no publications on the HTC process utilizing $FeCl_3$ catalyst on avocado peels have been published to date. This work systematically examines the influence of reaction parameters (reaction temperature, reaction time, catalyst/feedstock ratio) on the characteristics of the hydrochars produced. The obtained research results open the way to apply the HTC process to convert cheap biomass into energy-rich solid fuel, enhance the value of agro-industrial by-products, bring various economic benefits, and contribute to environmental protection.

2. Experimental

2.1. Materials. Avocado peels were locally collected in Daklak (12°45′59″N 108°19′31″E) in Vietnam. First, distilled water was used to rinse the avocado peel in order to get rid of dirt and other inorganic impurities. Subsequently, avocado peels were dried at 105°C for 48 h in order to be later crushed and sifted to obtain a uniform powder of about 300 μm. The powdered material was stored in a sealed glass bottle and in a dry, cool, and dark place.

Ferric chloride hexahydrate ($FeCl_3.6H_2O$, 99%) was bought from Sigma Aldrich. Deionized (DI) water owning a resistivity of 18 MΩ·cm was used in all experiments.

2.2. Hydrothermal Carbonization Treatment Experiment. The HTC process was conducted in a high-pressure stirred laboratory reactor (Parker Autoclave Engineers). Experimentally, a powder of avocado peel (100 g) and deionized water (600 mL) were mixed in the reactor. HTC experiments of avocado peel were carried out at different reaction temperatures (180, 200, and 220°C) for 5 h in the presence of $FeCl_3$ catalyst (catalyst/feedstock ratio of 20% by weight). The reaction mixture was stirred at room temperature for 20 minutes at 400 rpm, then heated to the desired temperature at a heating rate of 4°C·min^{-1}. Similarly, the effect of various reaction times (3, 5, 12, 18, and 24 h) on the HTC process of avocado peel was tested at 220°C with a catalyst/feedstock mass ratio of 20%. Besides, the various catalyst/feedstock mass ratios of 5, 10, 15, 20, and 25% were also studied at 220°C for 5 h to evaluate the role of the $FeCl_3$ catalyst. At the end of the reaction, the reactor was let cool to room temperature, and the solid products were separated by filtration and washed several times with deionized water until pH neutral. The washed solid product was dried at 105°C for 24 h.

Table 1 displays a list of produced samples, in which the produced hydrochar is denoted in the form "x-y-z," where x is the reaction temperature, y is the reaction time, and z is the catalyst/feedstock ratio. For example, if hydrochar is obtained from the reaction at 220°C for 5 h with a catalyst/feedstock mass ratio of 20% will be denoted as "220-5-20."

2.3. Characterization Methods. The surface morphology and microstructure of hydrochars were investigated by using scanning electron microscopy (SEM) and electron dispersive X-ray (EDX) analysis (Hitachi S-4800 FESEM with Horiba EDX system). A Nicolet 6700 Thermo Fisher was utilized to record Fourier Transform Infrared spectroscopy (FT-IR). Elemental compositions (C, H, O, N, and S) were determined according to ASTM D3176-15 by using a Perkin-Elmer Analyzer 2400 Series II.

Thermogravimetric analysis (TGA) and differential thermogravimetric (DTG) were carried out on a Diamond TG/DTA analyzer (Perkin Elmer Instruments). Combustion behaviors of feedstock and obtained hydrochars were determined by heating from room temperature to 900°C with a heating rate of 10°C·min^{-1} under an air atmosphere. At this temperature, the ash content (ash—wt%) in the samples was determined through the residual solid content after the TGA measurement. On the other hand, proximate analysis was determined through a similar thermal program but was performed under an argon flow [27]. In which the moisture content (MC) and the volatile fraction (VM–wt%) were determined based on the respective loss of mass in the heating range from room temperature to 150°C and from 150°C to 600°C.

In addition, TG and DTG profiles provided data to determine ignition temperature (T_i), burnout temperature (T_b), and temperature peaks via the intersection method [28]. The first one, point A, can be seen in Figure 1, where the TGA curve and a vertical line from the first DTG peak represent the highest value cross. Point B was where devolatilization started. T_i was the intersection point of the tangent at A on the TGA curve and the horizontal line through B. Meanwhile, T_b was the temperature at which the weight loss was constant.

2.4. Analytical Approach. The following formula was used to compute the yield of produced hydrochars:

$$\text{Hydrochar yield}\,(\%) = \left(\frac{\text{mass of hydrochar}}{\text{mass of raw material}}\right) \times 100\%. \quad (1)$$

The expression (1) calculates all mass values for dry materials.

The fixed carbon content (FC–wt%) was calculated using the following formula based on the TG-DTA analytical results [27]:

Table 1: Hydrochar yield and elemental analysis of feedstock and different hydrochars.

Samples	Hydrochar yield (%)	Ultimate analysis (wt%)					Atomic ratio	
		C	H	O	N	S	H/C	O/C
Avocado peel	—	46.16 ± 0.32	6.05 ± 0.06	43.01 ± 0.05	1.83 ± 0.010	1.64 ± 0.056	1.57 ± 0.022	0.70 ± 0.006
180-5-20	62.7 ± 0.30	63.48 ± 0.48	5.40 ± 0.04	29.31 ± 1.49	0.53 ± 0.026	0.22 ± 0.044	1.02 ± 0.015	0.35 ± 0.011
200-5-20	58.1 ± 0.17	65.13 ± 0.15	4.91 ± 0.03	27.21 ± 0.33	0.81 ± 0.061	0.62 ± 0.139	0.90 ± 0.006	0.31 ± 0.009
220-3-20	54.5 ± 0.36	65.25 ± 0.26	4.71 ± 0.07	27.13 ± 0.68	0.99 ± 0.004	0.65 ± 0.062	0.87 ± 0.003	0.31 ± 0.010
220-5-20	54.2 ± 0.78	67.15 ± 0.45	4.63 ± 0.09	25.46 ± 0.34	0.86 ± 0.050	0.87 ± 0.085	0.83 ± 0.019	0.28 ± 0.012
220-12-20	53.8 ± 0.17	69.36 ± 0.25	4.65 ± 0.58	24.58 ± 0.42	0.58 ± 0.004	0.37 ± 0.092	0.80 ± 0.103	0.27 ± 0.011
220-18-20	53.6 ± 0.36	66.09 ± 0.57	4.62 ± 0.17	26.59 ± 0.24	0.69 ± 0.046	0.58 ± 0.061	0.84 ± 0.038	0.30 ± 0.003
220-24-20	52.9 ± 0.36	65.77 ± 0.34	4.91 ± 0.16	25.81 ± 0.41	1.17 ± 0.011	0.98 ± 0.070	0.90 ± 0.027	0.29 ± 0.012
220-5-0	60.5 ± 0.26	56.50 ± 1.02	5.07 ± 1.21	36.12 ± 0.68	0.84 ± 1.091	0.61 ± 0.046	1.08 ± 0.030	0.48 ± 0.017
220-5-5	52.1 ± 0.26	63.37 ± 0.90	4.97 ± 0.09	27.76 ± 0.26	1.87 ± 0.070	1.02 ± 0.062	0.94 ± 0.018	0.33 ± 0.004
220-5-10	53.8 ± 0.10	64.99 ± 0.84	4.98 ± 0.16	25.98 ± 0.34	1.85 ± 0.044	1.02 ± 0.599	0.92 ± 0.037	0.30 ± 0.007
220-5-15	52.5 ± 0.26	66.18 ± 0.21	4.91 ± 0.38	25.92 ± 0.22	1.18 ± 0.044	0.89 ± 0.207	0.89 ± 0.072	0.29 ± 0.008
220-5-25	53.3 ± 0.17	65.74 ± 0.22	4.86 ± 0.24	25.20 ± 0.46	1.77 ± 0.046	1.16 ± 0.095	0.89 ± 0.041	0.29 ± 0.003

Data are shown as the mean ± SD ($n = 3$).

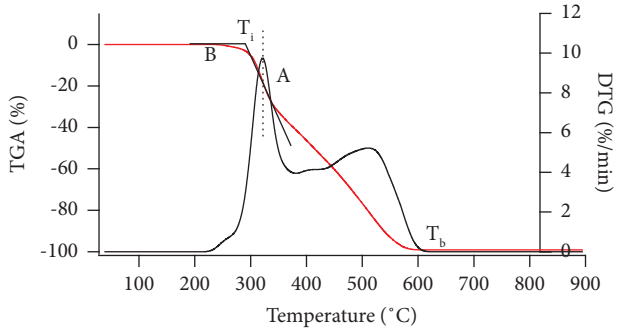

Figure 1: Schematic of determining T_i and T_b from the intersection method.

$$\mathrm{FC}(\%) = 100\% - \mathrm{MC}(\%) - \mathrm{VM}(\%) - \mathrm{Ash}(\%). \quad (2)$$

The high heating value (HHV) was determined using the Channiwala and Parikh (3) formula, which is well-known for its accuracy [29].

$$\mathrm{HHV}\left(\mathrm{MJ}kg^{-1}\right) = 0.3491C + 1.1783H + 0.1005S - 0.1034O - 0.0151N - 0.0211\mathrm{Ash}, \quad (3)$$

where C, H, O, N, S, and ash were the content (wt%) of carbon, hydrogen, oxygen, nitrogen, sulfur, and ash, respectively.

All experiments were carried out in triplicate. The results were presented as a mean and standard deviation (SD).

3. Results and Discussion

3.1. Structural Properties of Hydrochar. The morphology of the avocado peel material and the hydrochar samples produced under different conditions were observed by using scanning microscopy and are presented in Figures 2–4. Figure 2 shows that granules appear in many different shapes, but mostly oval, on the avocado peel material. These granules are 10–20 μm in diameter with a rough surface (Figures 2 and 3) and have an indent at one end, which disperses individually with a thick surface density. A similar characteristic result is also found in the SEM analysis of the avocado extract [30, 31].

After the HTC process, there was a significant change in the surface morphology of the hydrochar. At 180°C, the obtained hydrochar surface (sample 180-5-20) became spongier, and a few microspheres with diameters of 1 to 1.7 μm began to appear sparsely. The results of the EDX analysis (not shown here) show that the composition of these spheres is carbon. When continuing to increase the temperature to 200°C, the hydrochar surface was still an alternation of single spheres between porous structures, but the density of the spheres began to increase remarkably. When the reaction temperature increased to 220°C, the surface of the material was mainly composed of carbon microspheres with smooth surfaces and large diameters in the range of 1.5–4 μm.

Figure 3 shows the change in the surface structure of hydrochars obtained at different reaction times. After 3 hours of reaction, a few small spheres with sizes ranging from 0.5 to 1.5 μm dispersed singly, interspersed with debris. When raising the reaction time to 5 h, it was noticed that the carbon spheres' size had increased, and their surfaces had become smoother. The microsphere carbon structure disappeared when the reaction time continued to be extended to 12 h, at which time the hydrochar sample had a structure like large "patches of psoriasis" and was almost unchanged despite increasing the reaction time up to 24 h. These wide plates are the result of the agglomeration of carbon microspheres and the aggregation of porous structures as the reaction time is prolonged [10].

Figure 4 manifests the SEM images of hydrochars with different catalyst/feedstock ratios. It is easy to see that the sample without catalyst (220-5-0) has the same surface morphology as the material sample, with a very small amount of spherical carbon, about 2.5 μm in size. When increasing the catalyst/feedstock ratio to 5%, the number of microspheres increased significantly with diameters ranging from 0.5–1.5 μm, scattering among porous structures on the surface of hydrochars. The presence of $FeCl_3$ catalyst makes

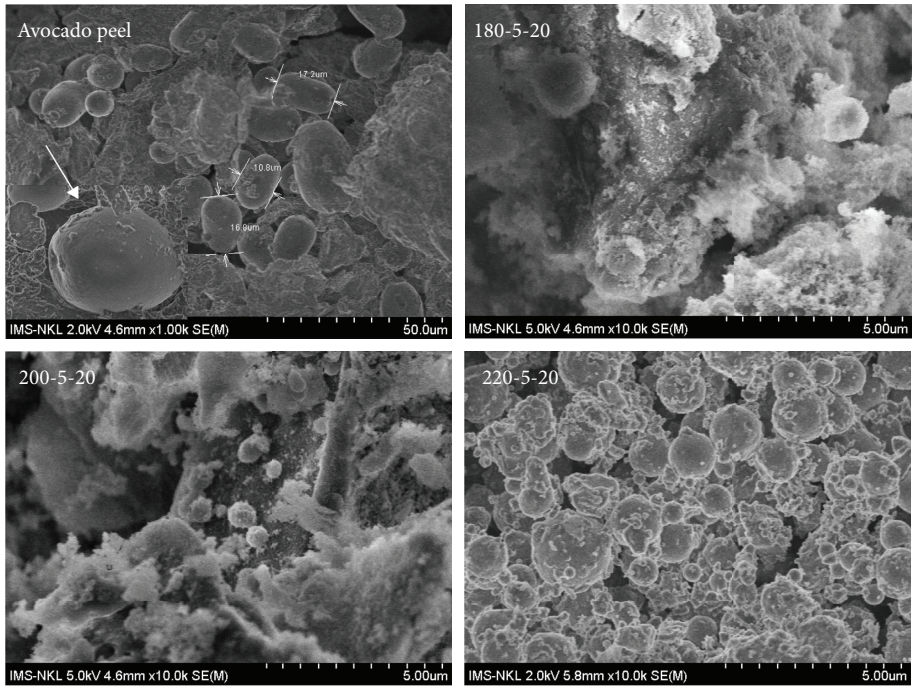

Figure 2: SEM images of feedstock and hydrochars at different temperatures.

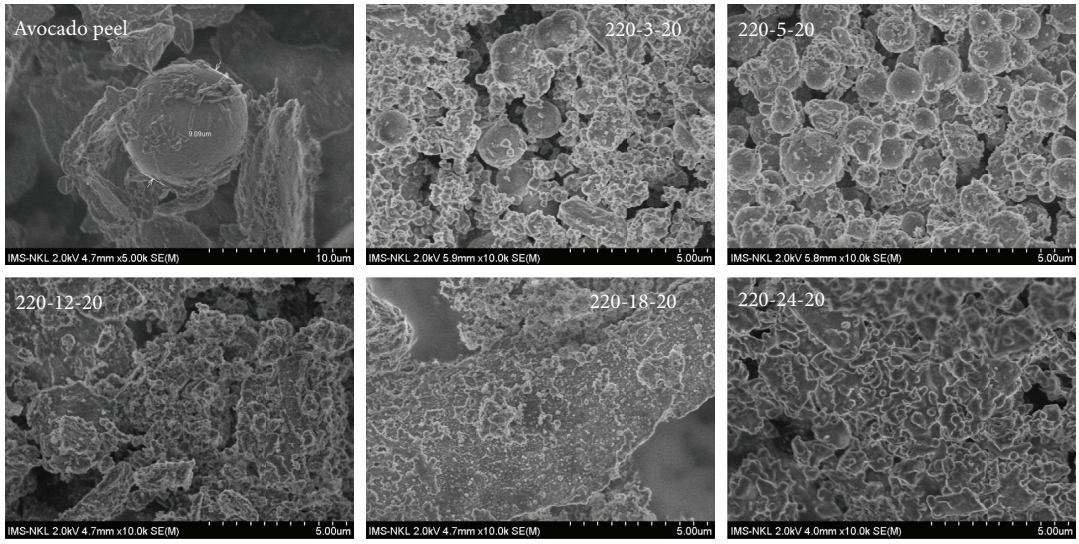

Figure 3: SEM images of hydrochars at different reaction times.

the reaction medium more acidic—a favorable condition that hastens the hydrolysis reaction and enhances the formation of microspheres in the initial stage of the reaction [32]. Continuing to the increasing amount of catalyst led to increasing the density of the spheres, and when the catalytic ratio reached 25%, in addition to the carbon spheres of various sizes, many small fragments were overlapping. A similar formation of carbon-rich spheres was also observed during the HTC of starch and rice in the presence of iron oxide or $[Fe(NH_4)_2(SO_4)_2]$ catalyst [24].

The FT-IR spectra of the feedstock (Figure S1) shows the main absorption peaks located at 3600–3200 cm^{-1} (O-H), 2950–2800 (C-H), 1725 cm^{-1} (C = O), 1605 cm^{-1} (C = C), 1515 cm^{-1} (C = C), 1450 cm^{-1} (C-H), and 1245–1000 cm^{-1} (C-O). After the HTC process, the FTIR spectrum of the hydrochars had a lot of changes compared to the raw avocado peel (Figures S2 and S3). Specifically, for produced hydrochar (Figures S2–S4), the signal intensities of the absorption bands at ~3600–3200 cm^{-1}, 2950–2800 cm^{-1}, 1725 cm^{-1}, and 1460–1000 cm^{-1} experience sharp declines, which indicates that dehydration has occurred, which is also consistent with the decrease in O/C and H/C ratios as shown in Table 1. On the other hand, it is easy to see the disappearance of two peaks at 1725 and 1245 cm^{-1}, respectively, to

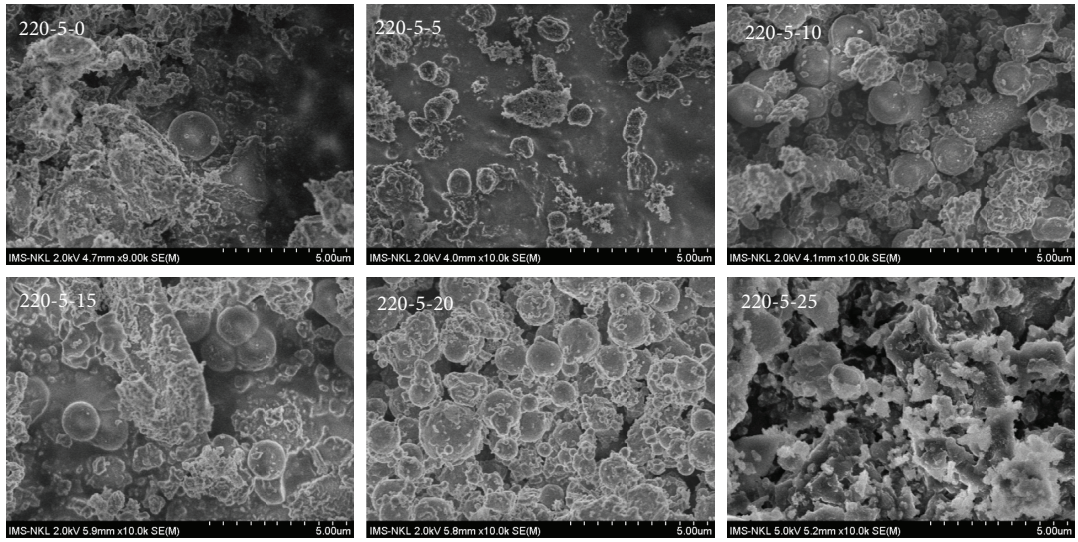

Figure 4: SEM images of hydrochars at different catalyst/feedstock ratios.

C = O and C-O stretching vibrations, which is caused by the breaking of ester bonds in hemicellulose [33]. At the same time, two new, low-intensity absorption peaks appeared at ~1700 and 1210 cm^{-1}, attributed to the C = O and C-O stretching vibrations in the spectrum of produced hydrochars.

The signal intensity variation on the spectrum of obtained hydrochars indicates that at low-temperature, hemicellulose, cellulose, and a part of lignin are seen to be decomposed first when the reaction conditions become more severe, and a long enough reaction time will cause lignin to be more strongly decomposed. Indeed, this shows that the signal intensities of two peaks at 1020 cm^{-1}, ascribed to the C-O stretching vibrations in cellulose and lignin in the feedstock, slowly reduced and vanished completely after 220°C and 12 h or an increase in the catalyst/feedstock ratio to 10%. Similarly, the decrease in the signal intensity of the peak at position 1515 cm^{-1} related to the C = C bond in the aromatic skeleton of lignin was observed with increasing reaction temperature and time (Figures S2 and S3). Meanwhile, the signal intensity of the absorption peak at about 1450 cm^{-1} position corresponding to C-H deformation in carbohydrate and lignin increased. This phenomenon was also witnessed during the HTC process of corn stalk [34].

The formation of C = C bonds in the aromatic ring structure was also confirmed by the appearance of C-H bending vibrations and C = C stretching vibrations at the 750–875 and 1605 cm^{-1} absorption bands, respectively. Among the surveyed parameters, Figure S2 shows that the reaction temperature has the most significant influence on the formation/recombination of aromatic ring structures.

3.2. Chemical and Energetic Properties of Hydrochar

3.2.1. Hydrochar Yield and Chemical Properties of Hydrochar. The results presented in Table 1 show that the solid mass yield decreases significantly with increasing temperature but only slightly decreases when the reaction time is extended. Meanwhile, the effect of the catalyst/feedstock ratio is not clear. This phenomenon was also observed in previous publications [35, 36], which showed that when the reaction temperature increases, a change in autogenous pressure happens, which changes the viscosity of water. As a result, thereby facilitating the penetration process and destroying the biomass structure. Consequently, feedstock solubilization becomes more efficient, resulting in a decrease in solid recovery.

Solid mass yield is less variable when changing reaction time. This is explained thanks to the breakdown of long-chain compounds in feedstock that took place right in the heating phase [36]. When the desired temperature is reached, the process continues. However, the results in Table 1 show that, after about 5 hours of reaction, the solid mass yield hardly changes anymore. Compared to the temperature and reaction time, the catalyst/feedstock ratio has a similar but not clear effect on hydrochar yield when the ratio increases from 5 to 25%. It is easy to see that all samples that use $FeCl_3$ catalyst give hydrochar yields of 52 to 54%; meanwhile, the noncatalytic sample (220-5-0) has a much higher yield, 60.5%. This phenomenon can be ascribed to the presence of $FeCl_3$—one kind of Lewis acid which is able to promote graphitization and polymer crosslinking [37]. In addition, according to these authors [37–39], thanks to the ability of Lewis acids to accept electrons, the breaking of C-O, C-H bonds and the formation of C = C bonds become more favorable. As a result, the O and H content in the hydrochar decreased sharply. Contrarily, the sample without using a catalyst had a slight decrease in oxygen content, leading to the recovery efficiency of a solid product being significantly higher.

Table 1 and the Van Krevelen diagram in Figure 5 show the variation in atomic ratio O/C and H/C calculated based on the results of elemental analysis. The Van Krevelen diagram clearly shows the change in the O/C and H/C atomic ratios when converting from raw materials to hydrochar, followed by two main reaction trends, dehydration and decarboxylation, similar to the HTC process for other

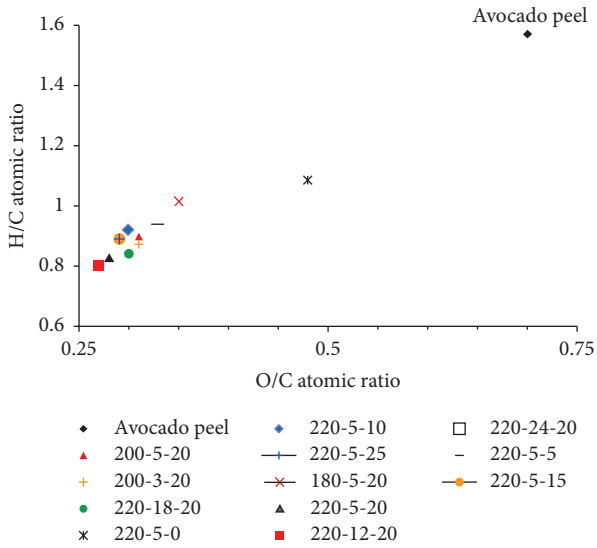

Figure 5: Van Krevelen diagram of feedstock and hydrochar samples.

biomass such as corncob residual [33], and tobacco stalk [40]. Compared with raw avocado peel, the ratio of O/C and H/C in hydrochar decreased remarkably with increasing reaction temperature and reached the lowest values of 0.27 and 0.80, respectively, for samples 220-12-20. In contrast, at this same temperature, after 5 h of reaction, the noncatalytic sample (sample 220-5-0) gave the highest O/C and H/C ratios among the obtained hydrochars, 0.48 and 1.08, respectively. Also, it is easy to see that at 220°C, when the reaction time was extended, or the amount of catalyst was changed, the O/C ratio was almost unchanged (~0.29), while the H/C ratio had a slight variation (0.80–0.90). The Van Krevelen diagram also shows that the HTC process of avocado peel occurs almost completely after 5 h of reaction at 220°C in the presence of an $FeCl_3$ catalyst.

The elemental compositions of the raw material and produced hydrochars are shown in Table 1. It is easy to see that, after the HTC process, the carbon content in the hydrochars increased sharply, especially with the catalytic sample group (up to about 20%). This demonstrates the role of $FeCl_3$ in creating an acidic environment that is favorable for the decomposition of macromolecules in biomass components.

The results displayed in Table 1 show that high reaction temperature promotes biomass decomposition and moisture removal better than retention time; hence, hydrochar yield is mainly influenced by temperature. In contrast, retention time affects more pronouncedly C content than reaction temperature because the longer the reaction time is, the more favorable the carbon enrichment in hydrochar is, leading to an increase in C content but a significant decrease in O content. These results are completely consistent with previous studies [36, 38]. Sample 220-12-20 shows the highest C content of 69.36%. When the reaction time is longer than 12 h, the carbon content begins to decrease, which is explained by the fact that more liquid and gaseous products are produced when the reaction time is prolonged [36].

3.2.2. Energetic Properties of Hydrochar. The results of proximate analysis of the avocado peel and hydrochars are presented in Table 2. It is easy to see that the HHV of all hydrochar samples (22–27 $MJ{\cdot}kg^{-1}$) rose notably compared to avocado peel (18.91 $MJ{\cdot}kg^{-1}$). The HHV increases with temperature increasing from 180 to 220°C and reaction time increasing to 12 h. Compared with temperature, the reaction time and catalyst content had a more pronounced effect on HHV. It can be easily observed that HHV increased rapidly as the reaction time increased from 1 to 5 h. After 5 h of reaction, this value increased slowly and even tended to decrease slightly after 12 h of reaction. In particular, when comparing produced hydrochar at the same temperature of 220°C and 5 h of reaction, the noncatalytic 220-5-0 sample gave significantly lower HHV than the corresponding values of the other hydrochars by using $FeCl_3$ catalyst. This result once again confirms the role of $FeCl_3$ in the formation of an acidic environment. This is a favorable environment for water to act as a polar organic solvent that helps promote decarboxylation and dehydration more efficiently [32, 41, 42] and enhances carbonization [36, 37]. As a result, the carbon content of the produced hydrochar increased. All these factors contribute to the HHV of hydrochars produced from avocado peel being more significantly enhanced than that of other biomass types [15, 17, 36].

The proximate analysis results in Table 2 show that when the reaction temperature and the catalyst/feedstock ratio increase, the volatile matter of hydrochar decreases, and the fixed carbon content increases significantly. Meanwhile, the ash content in raw materials and hydrochar samples almost has no change (only about 1.3%) even when the reaction temperature increases. According to the authors [43, 44], in the HTC process, a part of the volatile matter will be transformed into a gas phase product such as CO_2, and the rest participates in the repolymerization reaction to increase the fixed carbon content, improving the quality of the obtained hydrochars. When increasing the reaction time from 5 h to 12 h, FC content does not increase much. Especially when the reaction time was extended further, the FC content hardly changed. This demonstrates that the transformation and material structure rearrangements mainly occurred in the first 5 h and were stable since 12 h of reaction. This hypothesis is also consistent with the results of hydrochar structure analysis, such as FT-IR, SEM, and element analysis results.

Combustion behaviors of avocado peel and hydrochars were analyzed by using TGA in the air atmosphere. Their TG-DTG curves are shown in Figures S5–S10, and the resulting combustion parameters are displayed in Table 3. An ignition temperature (T_i) is described as the lowest temperature at which fuel ignites spontaneously in a normal atmosphere without an external ignition source. Meanwhile, burnout temperature (T_b) is the temperature at which fuel is almost completely consumed. Ignition and burnout temperatures are two of the most important properties that directly affect fuel use.

It can be easily noticed that the T_i and the T_b of hydrochar both increased compared to the avocado peel materials. As the temperature and reaction time increase, T_i

Table 2: Results of proximate analysis for feedstock and different hydrochars.

Samples	Proximate analysis (wt%)				HHV (MJ kg^{-1})
	MC	VM	Ash	FC	
Avocado peel	4.11 ± 0.08	65.38 ± 1.08	1.31 ± 0.070	29.20 ± 2.11	18.91 ± 0.03
180-5-20	2.46 ± 0.30	60.61 ± 1.07	1.30 ± 0.121	35.63 ± 0.29	25.48 ± 0.36
200-5-20	2.58 ± 0.13	54.68 ± 0.47	1.32 ± 0.589	41.42 ± 1.03	25.73 ± 1.32
220-3-20	3.04 ± 0.12	52.63 ± 0.36	1.20 ± 0.480	43.13 ± 0.84	25.55 ± 0.65
220-5-20	3.26 ± 0.48	48.84 ± 1.27	1.27 ± 0.024	48.21 ± 1.34	26.31 ± 0.51
220-12-20	2.27 ± 0.08	48.65 ± 0.67	1.23 ± 0.262	47.85 ± 0.38	27.15 ± 0.70
220-18-20	1.58 ± 0.16	50.43 ± 1.24	1.45 ± 0.126	46.54 ± 1.09	25.78 ± 0.54
220-24-20	2.56 ± 13.08	49.73 ± 0.04	1.36 ± 0.736	46.35 ± 1.09	26.13 ± 0.74
220-5-0	3.06 ± 0.21	62.43 ± 0.93	1.02 ± 0.061	33.49 ± 0.22	21.99 ± 0.81
220-5-5	1.36 ± 0.07	58.41 ± 0.51	1.08 ± 0.359	39.15 ± 1.19	25.17 ± 1.05
220-5-10	1.34 ± 0.10	57.29 ± 0.88	1.26 ± 0.166	40.11 ± 0.73	25.92 ± 0.67
220-5-15	1.65 ± 0.07	53.01 ± 1.33	1.33 ± 0.093	44.01 ± 0.21	26.25 ± 0.69
220-5-25	1.81 ± 0.06	57.52 ± 0.95	1.27 ± 0.183	39.40 ± 1.94	26.13 ± 1.07

Data are shown as the mean ± SD ($n = 3$).

Table 3: Combustion parameters of feedstock and different hydrochars were obtained from TGA analysis.

Samples	T_i (°C)	Stage 2		Stage 3		T_b (°C)
		T_2 (°C)	Weight loss (%)	T_3 (°C)	Weight loss (%)	
Avocado peel	248.32	291.98	54.98 ± 0.30	446.42	39.60 ± 0.54	622.19
180-5-20	282.39	320.02	38.54 ± 0.87	509.82	58.53 ± 1.35	656.36
200-5-20	281.52	315.89	30.27 ± 1.11	492.84	65.83 ± 0.68	653.30
220-3-20	281.34	316.36	28.31 ± 0.97	503.24	70.03 ± 0.23	651.28
220-5-20	283.13	317.94	26.56 ± 0.82	479.81	69.81 ± 1.11	662.17
220-12-20	278.64	312.22	26.14 ± 0.19	480.92	70.36 ± 0.25	668.46
220-18-20	279.78	310.24	26.83 ± 1.18	478.48	70.14 ± 1.37	658.39
220-24-20	282.24	312.86	26.27 ± 0.37	495.83	69.81 ± 0.55	673.67
220-5-0	274.08	321.29	42.51 ± 0.74	514.26	54.43 ± 0.74	618.50
220-5-5	286.70	315.93	36.14 ± 1.11	436.10	61.42 ± 0.59	626.53
220-5-10	284.28	308.52	31.69 ± 0.48	458.01	65.71 ± 9.80	639.51
220-5-15	285.89	310.81	27.88 ± 0.83	476.80	69.14 ± 1.05	646.27
220-5-25	294.08	312.14	27.13 ± 0.27	481.05	69.79 ± 0.46	658.83

Data are shown as the mean ± SD ($n = 3$).

also increases gradually. This is explained by the fact that when the temperature and the reaction time increase, the porous structure and specific surface area of the hydrochar decrease, thereby reducing the interaction between oxygen and organic matter [45], resulting in a gradual increase in ignition temperature. This result is completely in keeping with the SEM results analyzed above.

Compared to the temperature and reaction time, the catalyst/feedstock ratio shows the clearest influence on the T_b of produced hydrochars. When the ratio increased from 0 to 25%, T_b increased from 618.5°C to 658.83°C. This is explained by the presence of catalysts in the HTC process which facilitates the repolymerization of small molecular fragments while promoting aromatization to form aromatic ring compounds, increasing the FC content [37, 38] therefore expanding the T_b value over raw materials and noncatalytic samples.

TG-DTG curves show that all samples consisted of three main stages of mass change. The first stage of weight loss occurs when the room temperature is heated to 150°C, corresponding to moisture removal. Weight loss during this period is not much, and there is almost no difference between obtained hydrochars (only about 4% for raw material and 1.5–3% for hydrochars). The next temperature range from 200°C to 650°C takes place through a weight loss for all samples; it consists of two consecutive stages corresponding to devolatilization and decomposition of hemicellulose and cellulose (stage 2: 200–400°C) and chars combustion phase (stage 3: 400–650°C) [46].

In the temperature range of 200–650°C, it is easy to see that the TG curves of all hydrochars obtained at a temperature of more than 200°C in the presence of $FeCl_3$ catalyst had similar forms and slopes, were not clearly separated into two stages of weight loss (Figures S5, S7, and S9). Corresponding to their DTG curves (Figures S6, S8, and S10), only one shoulder peak (dashed arrows) appeared, which was a superposition of two-component peaks corresponding to stage 2 and stage 3. Within the temperature range of 200–400°C, the raw avocado peel decomposed most strongly, corresponding to a peak appearing at position T_2~292°C (significantly lower than T_2 of obtained hydrochars). Similar peaks can only be observed on the DTG curves of two samples, 180-5-20 and 220-5-0 (Figures S6 and S10), but at higher temperatures (~320°C). This is also shown clearly by

the slope of their TG curves in Figures S5 and S9. This phenomenon is explained by the low reaction temperature (180°C), or when the $FeCl_3$ catalyst is not used, the hydrolysis of cellulose and hemicellulose is incomplete. Therefore, for two samples, 180-5-20 and 220-5-0, their content that has not completely reacted in hydrochar was higher, causing the weight loss in stage 2 to occur more strongly than in the remaining hydrochars. This result is completely consistent with the results of calculating the hydrochar yield in Table 1 because the hydrochar yield of 180-5-20 and 220-5-0 is the highest among the surveyed samples. The influence of reaction time on the decomposition rate of hydrochar in stage 2 (Figures S7 and S8) was noted but not as noticeable as the reaction temperature or the catalyst/feedstock ratio.

For stage 3 (400–650°C), when reaction time and catalyst/feedstock ratio elevated, the weight loss and peak temperature (T_3) evidently increased. As previously analyzed, the more severe HTC conditions and the presence of $FeCl_3$ catalyst helped increase fixed carbon content in hydrochar, so the burning process at 400–650°C is directly related to the oxidation process of fixed carbon, which also drastically increased, resulting in that T_3 and T_b visibly expand (Table 3). This result is consistent with the analysis results of C content (Table 1) mentioned above.

4. Conclusion

The investigation of experimental parameters, such as reaction temperature (180–220°C), reaction time (3–24 h), and catalyst/feedstock ratio (0–25%) that influence the structure, chemical composition, and combustion characteristics of hydrochars obtained from hydrothermal carbonization of the avocado peel with the presence of $FeCl_3$ catalyst, has been systematically executed. The higher heating value increased from 18.91 $MJ{\cdot}kg^{-1}$ in the feedstock to the maximum value of 27.15 $MJ{\cdot}kg^{-1}$, corresponding to hydrochar, which is produced at 220°C for 12 h with 20% $FeCl_3$ catalyst (220-12-20). At the same time, the O/C and H/C ratios decreased remarkably because of the increasing dehydration and decarboxylation reactions at higher reaction temperatures and longer retention times. These almost unchanged ratios indicate nearly complete avocado peel conversion after 5 h of reaction at 220°C. At last, the TGA analysis shows that as the reaction time and the catalyst/feedstock ratio increase, T_i and T_b are enlarged; the weight loss and peak temperature T_3 (corresponding to the combustion phase) increase. With these thermal properties, hydrochar obtained from the HTC process for avocado peel can be applied as an energy-rich solid fuel. The obtained results open the potential application of the HTC process on inexpensive feedstocks on an industrial scale. This helps to expand the value of biomass resources and partially solves environmental pollution.

Data Availability

The datasets used and analyzed during the current study are available from the corresponding author upon request.

Conflicts of Interest

The authors declare that they have no conflicts of interest.

Acknowledgments

This research is funded by Vietnam National Foundation for Science and Technology Development (NAFOSTED) under grant number: 03/2018/TN.

Supplementary Materials

Figure S1: FTIR spectrum of the raw avocado peel. Figure S2: FTIR spectra of hydrochars produced at different reaction temperatures. Figure S3: FTIR spectra of hydrochars produced at different reaction times. Figure S4: FTIR spectra of hydrochars produced with different catalyst/feedstock ratios. Figure S5: TG curves of avocado peel and hydrochars obtained at different reaction temperatures. Figure S6: DTG curves of avocado peel and hydrochars obtained at different reaction temperatures. Figure S7: TG curves of avocado peel and hydrochars obtained at different reaction times. Figure S8: DTG curves of avocado peel and hydrochars obtained at different reaction times. Figure S9: TG curves of avocado peel and hydrochars obtained at different catalyst/feedstock ratios. Figure S10: DTG curves of avocado peel and hydrochars obtained at different catalyst/feedstock ratios. (*Supplementary Materials*)

References

[1] M. C. García-Vargas, M. D. M. Contreras, and E. Castro, "Avocado-Derived biomass as a source of bioenergy and bioproducts," *Applied Sciences*, vol. 10, 2020.

[2] A. Mora-Sandí, A. Ramírez-González, L. Castillo-Henríquez, M. Lopretti-Correa, and J. R. Vega-Baudrit, "Persea americana agro-industrial waste biorefinery for sustainable high-value-added products," *Polymers*, vol. 13, no. 11, 2021.

[3] A. Del Castillo-Llamosas, P. G. del Río, A. Pérez-Pérez, R. Yáñez, G. Garrote, and B. Gullón, "Recent advances to recover value-added compounds from avocado by-products following a biorefinery approach," *Current Opinion in Green and Sustainable Chemistry*, vol. 28, Article ID 100433, 2021.

[4] F. Sánchez, K. Araus, M. P. Domínguez, and G. S. Miguel, "Thermochemical transformation of residual avocado seeds: torrefaction and carbonization," *Waste and Biomass Valorization*, vol. 8, no. 7, pp. 2495–2510, 2017.

[5] M. P. Elizalde-González, J. Mattusch, A. A. Peláez-Cid, and R. Wennrich, "Characterization of adsorbent materials prepared from avocado kernel seeds: natural, activated and carbonized forms," *Journal of Analytical and Applied Pyrolysis*, vol. 78, no. 1, pp. 185–193, 2007.

[6] K. Dejene, K. Siraj, and S. A. Kitte, "Kinetic and thermodynamic study of phenol removal from water using activated carbon synthesizes from avocado kernel seed," *International Letters of Natural Sciences*, vol. 54, pp. 42–57, 2016.

[7] C. Palma, L. Lloret, A. Puen, M. Tobar, and E. Contreras, "Production of carbonaceous material from avocado peel for its application as alternative adsorbent for dyes removal," *Chinese Journal of Chemical Engineering*, vol. 24, no. 4, pp. 521–528, 2016.

[8] R. Mallampati, L. Xuanjun, A. Adin, and S. Valiyaveettil, "Fruit peels as efficient renewable adsorbents for removal of dissolved heavy metals and dyes from water," *ACS Sustainable Chemistry & Engineering*, vol. 3, no. 6, pp. 1117–1124, 2015.

[9] J. A. Libra, K. S. Ro, C. Kammann et al., "Hydrothermal carbonization of biomass residuals: a comparative review of the chemistry, processes and applications of wet and dry pyrolysis," *Biofuels*, vol. 2, no. 1, pp. 71–106, 2011.

[10] Y. Gao, X. Wang, J. Wang et al., "Effect of residence time on chemical and structural properties of hydrochar obtained by hydrothermal carbonization of water hyacinth," *Energy*, vol. 58, pp. 376–383, 2013.

[11] C. He, A. Giannis, and J. Y. Wang, "Conversion of sewage sludge to clean solid fuel using hydrothermal carbonization: hydrochar fuel characteristics and combustion behavior," *Applied Energy*, vol. 111, pp. 257–266, 2013.

[12] A. A. Arie, H. Kristianto, H. Muljana, and L. Stievano, "Rambutan peel based hard carbons as anode materials for sodium ion battery," *Fullerenes, Nanotubes, and Carbon Nanostructures*, vol. 27, no. 12, pp. 953–960, 2019.

[13] B. Zhang, M. Heidari, B. Regmi et al., "Hydrothermal carbonization of fruit wastes: a promising technique for generating hydrochar," *Energies*, vol. 11, no. 8, pp. 2022–2114, 2018.

[14] A. Saning, S. Herou, D. Dechtrirat et al., "Green and sustainable zero-waste conversion of water hyacinth (Eichhornia crassipes) into superior magnetic carbon composite adsorbents and supercapacitor electrodes," *RSC Advances*, vol. 9, no. 42, pp. 24248–24258, 2019.

[15] C. Zhang, X. Ma, X. Chen et al., "Conversion of water hyacinth to value-added fuel via hydrothermal carbonization," *Energy*, vol. 197, Article ID 117193, 2020.

[16] N. Srilek and P. Aggarangsi, "Key characteristics of carbonized corncob through hydrothermal and pyrolysis conversion techniques for further activation," *International Journal of Engineering and Advanced Technology*, vol. 8, no. 5, pp. 1089–1098, 2019.

[17] K. Kang, S. Nanda, G. Sun et al., "Microwave-assisted hydrothermal carbonization of corn stalk for solid biofuel production: optimization of process parameters and characterization of hydrochar," *Energy*, vol. 186, Article ID 115795, 2019.

[18] M. Kurniati, D. Nurhayati, and A. Maddu, "Study of structural and electrical conductivity of sugarcane bagasse-carbon with hydrothermal carbonization," *IOP Conference Series: Earth and Environmental Science*, vol. 58, no. 1, Article ID 012049, 2017.

[19] X. Chai, H. He, H. Fan, X. Kang, and X. Song, "A hydrothermal-carbonization process for simultaneously production of sugars, graphene quantum dots, and porous carbon from sugarcane bagasse," *Bioresource Technology*, vol. 282, pp. 142–147, 2019.

[20] J. Wu, J. Yang, G. Huang, C. Xu, and B. Lin, "Hydrothermal carbonization synthesis of cassava slag biochar with excellent adsorption performance for Rhodamine B," *Journal of Cleaner Production*, vol. 251, Article ID 119717, 2020.

[21] P. Sangjumras, P. Udomsap, N. Kaewtrakulchai, A. Eiad-Ua, M. Fuji, and S. Chutipaijit, "Effects of transition metal during the hydrothermal carbonization on characteristics of carbon materials," *AIP Conference Proceedings*, vol. 2010, 2018.

[22] V. Saadattalab, X. Wang, A. E. Szego, and N. Hedin, "Effects of metal ions, metal, and metal oxide particles on the synthesis of hydrochars," *ACS Omega*, vol. 5, no. 11, pp. 5601–5607, 2020.

[23] S. H. Yu, X. J. Cui, L. L. Li et al., "From starch to metal/carbon hybrid nanostructures: hydrothermal metal-catalyzed carbonization," *Advances in Materials*, vol. 16, no. 18, pp. 1636–1640, 2004.

[24] X. Cui, M. Antonietti, and S. H. Yu, "Structural effects of iron oxide nanoparticles and iron ions on the hydrothermal carbonization of starch and rice carbohydrates," *Small*, vol. 2, no. 6, pp. 756–759, 2006.

[25] S. Bee, A. Hamid, S. J. Teh, and Y. S. Lim, "Catalytic hydrothermal upgrading of α -cellulose using iron salts as a," *Lewis Acid*, vol. 10, no. 3, pp. 5974–5986, 2015.

[26] N. Fechler, S.-A. Wohlgemuth, P. Jäker, and M. Antonietti, "Salt and sugar: direct synthesis of high surface area carbon materials at low temperatures via hydrothermal carbonization of glucose under hypersaline conditions," *Journal of Materials Chemistry*, vol. 1, no. 33, pp. 9418–9421, 2013.

[27] D. Kalderis, M. S. Kotti, A. Méndez, and G. Gascó, "Characterization of hydrochars produced by hydrothermal carbonization of rice husk," *Solid Earth*, vol. 5, no. 1, pp. 477–483, 2014.

[28] J. J. Lu and W. H. Chen, "Investigation on the ignition and burnout temperatures of bamboo and sugarcane bagasse by thermogravimetric analysis," *Applied Energy*, vol. 160, pp. 49–57, 2015.

[29] S. A. Channiwala and P. P. Parikh, "A unified correlation for estimating HHV of solid, liquid and gaseous fuels," *Fuel*, vol. 81, no. 8, pp. 1051–1063, 2002.

[30] T. B. Bahru, Z. H. Tadele, and E. G. Ajebe, "A review on avocado seed: functionality, composition, antioxidant and antimicrobial properties," *Chemical Science International Journal*, vol. 27, no. 2, pp. 1–10, 2019.

[31] D. M. Dos Santos, D. P. R. Ascheri, A. De Lacerda Bukzem, C. C. Morais, C. W. P. Carvalho, and J. L. R. Ascheri, "Propriedades físico-químicas do amido da semente de abacate (Persea Americana mill)," *Bol. Cent. Pesqui. Process. Aliment.*vol. 34, no. 2, 2016.

[32] J. L. Liang, Y. H. Liu, and J. Zhang, "Effect of solution pH on the carbon microsphere synthesized by hydrothermal carbonization," *Procedia Environmental Sciences*, vol. 11, pp. 1322–1327, 2011.

[33] L. Zhang, Q. Wang, B. Wang, G. Yang, L. A. Lucia, and J. Chen, "Hydrothermal carbonization of corncob residues for hydrochar production," *Energy & Fuels*, vol. 29, no. 2, pp. 872–876, 2015.

[34] S. Guo, X. Dong, T. Wu, F. Shi, and C. Zhu, "Characteristic evolution of hydrochar from hydrothermal carbonization of corn stalk," *Journal of Analytical and Applied Pyrolysis*, vol. 116, pp. 1–9, 2015.

[35] A. Funke, F. Ziegler, and T. U. Berlin, "Hydrothermal carbonization of biomass: a summary and discussion of chemical mecha- nisms for process engineering," *Biofuels Bioproducts and Biorefining*, vol. 4, pp. 160–177, 2010.

[36] S. Nizamuddin, H. A. Baloch, G. J. Griffin et al., "An overview of effect of process parameters on hydrothermal carbonization of biomass," *Renewable and Sustainable Energy Reviews*, vol. 73, pp. 1289–1299, 2017.

[37] Y. Cai, Y. Hu, L. Song et al., "Catalyzing carbonization function of ferric chloride based on acrylonitrile–butadiene–styrene copolymer/organophilic montmorillonite nanocomposites," *Polymer Degradation and Stability*, vol. 92, no. 3, pp. 490–496, 2007.

[38] T. Wang, Y. Zhai, Y. Zhu, C. Li, and G. Zeng, "A review of the hydrothermal carbonization of biomass waste for hydrochar formation: process conditions, fundamentals, and

physicochemical properties," *Renewable and Sustainable Energy Reviews*, vol. 90, pp. 223–247, 2018.

[39] M. Molina-Sabio and F. Rodríguez-Reinoso, "Role of chemical activation in the development of carbon porosity," *Colloids and Surfaces A: Physicochemical and Engineering Aspects*, vol. 241, no. 3, pp. 15–25, 2004.

[40] J. Cai, B. Li, C. Chen, J. Wang, M. Zhao, and K. Zhang, "Hydrothermal carbonization of tobacco stalk for fuel application," *Bioresource Technology*, vol. 220, pp. 305–311, 2016.

[41] N. Akiya and P. E. Savage, "Roles of water for chemical reactions in high-temperature water," *Chemistry Review*, vol. 102, no. 8, pp. 2725–2750, 2002.

[42] A. Kruse and N. Dahmen, "Water—a magic solvent for biomass conversion," *The Journal of Supercritical Fluids*, vol. 96, pp. 36–45, 2015.

[43] X. Zhuang, H. Zhan, Y. Huang, Y. Song, X. Yin, and C. Wu, "Denitrification and desulphurization of industrial biowastes via hydrothermal modification," *Bioresource Technology*, vol. 254, pp. 121–129, 2018.

[44] Y. Lin, X. Ma, X. Peng, S. Hu, Z. Yu, and S. Fang, "Effect of hydrothermal carbonization temperature on combustion behavior of hydrochar fuel from paper sludge," *Applied Thermal Engineering*, vol. 91, pp. 574–582, 2015.

[45] X. Zhuang, Y. Song, H. Zhan, X. Yin, and C. Wu, "Gasification performance of biowaste-derived hydrochar: the properties of products and the conversion processes," *Fuel*, vol. 260, Article ID 116320, 2020.

[46] C. Peng, Y. Zhai, Y. Zhu et al., "Production of char from sewage sludge employing hydrothermal carbonization: char properties, combustion behavior and thermal characteristics," *Fuel*, vol. 176, pp. 110–118, 2016.